ENGINEERING TRANSACTIONS • *Engng. Trans.* • **62**, 4, 313–328, 2014
Polish Academy of Sciences • Institute of Fundamental Technological Research (IPPT PAN)
National Engineering School of Metz (ENIM) • Poznan University of Technology

Nonlinear Finite Element Simulation of Friction Stir Processing of Marine Grade 5083 Aluminum Alloy

Emad Eldin M. KISHTA, Farid H. ABED, Basil M. DARRAS

College of Engineering, American University of Sharjah
Sharjah, UAE
e-mail: fabed@aus.edu

As friction stir processing is emerging as a new technique for material enhancement, full understanding of the process has not been achieved yet. The resulting mechanical and microstructural properties are controlled by processing parameters like rotational and translational speeds. To support experimental results, it is very necessary to develop robust finite element models that can simulate the friction stir welding process and predict the effect of the processing parameters on the thermal profiles. This, in turn, gives a forecast of the expected tensile and microstructural properties of the alloy used. This paper presents a thermomechanical-based finite element modeling adopting a coupled Eulerian Lagrangian formulation to simulate the friction stir process for Marine Grade AA5083. A set of friction stir welding tests considering different rotational and translational speeds is also conducted in this study to verify and validate the present FE modeling. The thermal profiles as well as the peak temperatures measured experimentally using infra-red imaging technique were successfully predicted by the proposed FE modeling.

Key words: friction stir processing, nonlinear finite element, Eulerian-Lagrangian formulation, temperature profile, aluminum.

1. Introduction

Friction stir processing (FSP) is an emerging material enhancement technique utilized from the solid-state welding technique known as friction stir welding which was invented by the welding institute [1]. FSP is done using a specially designed rotating tool that exerts heat through friction on the alloy causing the material to soften while being stirred. The stirring is considered a plastic deformation under a relatively low temperature causing dynamic recrystallization as well as grain growth. To be optimized as a material enhancement or grain refinement technique, the grain growth must be minimized by altering the rotational speed, feed rate and welding medium [2–5]. To have a better understanding of the problem and minimize experimental work, finite element models capable of

simulating the FSP are deemed necessary to predict the resulting thermal profile and large deformation at different rotational and translational speeds.

Various modeling techniques of FSP can be found in the literature [6–10]. Buffa *et al.* [11] used a continuum based 3-D Lagrangian formulation for modeling Friction Stir Welding (FSW) to predict the non-symmetric effective strain distribution across the weld line in addition to the symmetric temperature profile caused by the FSW process. Hamilton *et al.* [12] proposed an energy-based model with Johnson-Cook flow stress definition to predict the thermal profile during the FSW process. The model predicted the heat generation and maximum weld temperature at relatively higher rotational speeds, however, it underestimated the maximum weld temperature at the lower rotational speeds. Schmidt and Hattel [13] generated a thermo-mechanical model to analyze the conditions where FSW takes place perfectly and no voids occur on the weld line. The model was developed using ABAQUS/Explicit [14] with Arbitrary Lagrangian-Eulerian (ALE) formulation and remeshing technique to avoid excessive distortion in the mesh. Zhang and Zhang [15] developed a thermo-mechanical model using ALE formulation via ABAQUS/Explicit to predict the changes in thermal histories and material deformation in FSW under different welding parameters. The FE model showed that the welding temperature increases as the rotational speed increases. The increase in rotational speed resulted in increasing the power consumption and residual stresses in the sample. A 3D model produced by Ulysse [16] is used to predict the forces acting on the FSW tool. The model was developed using commercial software FIDAP, and experimental results were used to validate the model. The model achieved close results to those found in the experimental work but tended to over predict the temperature.

The main issue in modeling FSP is the high deformation that occurs during the process. Using finite element model based on full Lagrangian approach results in element distortion due to the high plastic deformation. The element distortion could be avoided using remeshing technique in ABAQUS, however, using this technique increases the computational time drastically and not always converges. Schmidt and Hattel [13] reported a computational time of 14 days to reach a steady-state after 10 seconds of simulation time. The only reported method to reduce the computational time was using mass scaling [15, 16], however, the computational time was still very high and the results were unrealistic in some cases. None of the above mentioned researches has discussed the difficulties encountered during the FE modeling of FSP using the ALE formulation approach.

In the present work, a 3-D coupled Eulerian-Lagrangian finite element model using ABAQUS/Explicit is developed, as an alternative to previous approaches, to predict the effect of processing parameters of FSP. The model is utilized to predict the temperature profiles during FSP at different input parameters.

A set of experimental FSW tests is also conducted to validate the proposed FE modeling at different rotational and translational speeds.

2. Experimental procedure

FSW samples of 5083 marine-grade Aluminum Alloy, with 130 mm length, 60 mm width and 5 mm thickness, were used in this study. The chemical composition of the AA083 is presented in Table 1. The experiment was performed using a CNC vertical machine with a specially-designed FSP tool with a featureless shoulder. The tool has a diameter of 15 mm and has a threaded pin with a 5 mm diameter and 4 mm length. The sample was clamped in the CNC machine using a locally designed and built set up. Moreover, the sample was plunged prior to FSP as it was proven to enhance the properties of the welded material [17]. The steel tool was then driven into the sample at different rotational speeds ranging from 600 to 900 rpm. The experimental set up and the tool used are shown in Fig. 1. K-type thermocouples were placed on the retreating and advancing sides of each specimen to record the temperature along the processing line as different temperatures were reported on each side. The placement of the thermocouples can be viewed in the schematic description presented Fig. 2.

Table 1. Chemical Composition (%) of Aluminum Alloy 5083.

Al	Cr	Cu	Fe	Mg	Al	Cr	Cu	Fe	Mg
Bal.	0.05–0.25	> 0.1	> 0.4	4–4.9	94.2–95.6	0.05–0.25	> 0.1	> 0.4	4–4.9

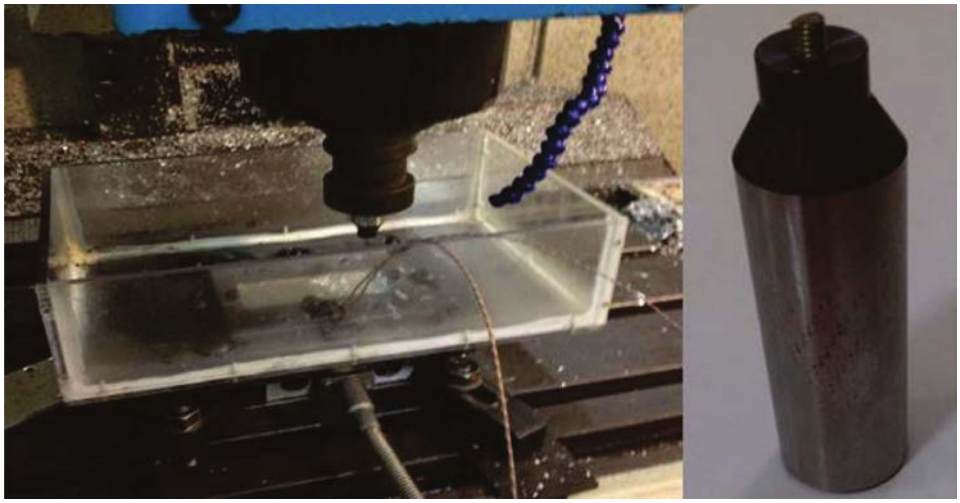

Fig. 1. Experimental setup.

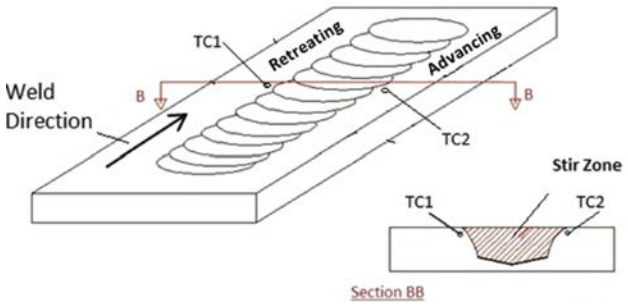

FIG. 2. Schematic diagram showing thermocouples placements.

Infra-red camera was used to record the temperature distribution at various locations on the surface and for different stages of FSP. As the tool is rotating and moving in the processing direction, the rotation of the tool acts in the same direction of the weld in the advancing side, while it acts in the opposite direction of the weld in the retreating side. This movement causes the temperature in the advancing side to increase further and the material to be moved from the retreating to the advancing side. Figure 3 shows an experimental FSP sample with excess material appearing on the advancing side with indications of the welding and rotational directions.

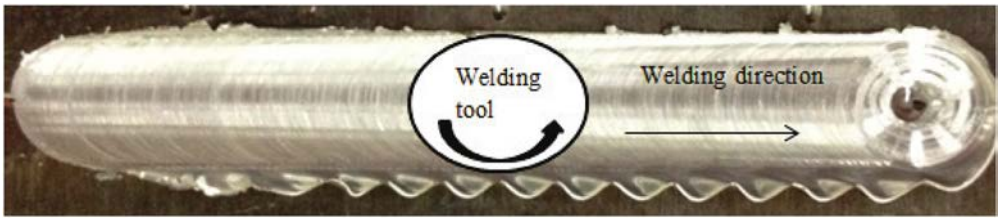

FIG. 3. FSP sample showing excess material on the advancing side and rotational and welding direction of the tool.

3. FINITE ELEMENT FORMULATION

3.1. Governing equations

The present FE modeling accounts for two types of heat generation during FSP; the first is due to plastic deformation, r^{pl} and the second is due to friction, q. To measure the heat generated due to friction, the following equation for the heat flux density was adopted:

$$q = q_k + q_r - f q_g, \tag{3.1}$$

where q_k is the heat flux due to conduction, q_r is the heat flux due to radiation, f is the fraction of heat generated into the surface and q_g is the heat flux produced by the interface element due to frictional heat generation.

The heat flux due to friction is defined as follows:

$$q_k = k\Delta T, \tag{3.2}$$

in which k is the heat transfer coefficient and ΔT is the temperature difference between the two surfaces. The heat transfer coefficient is dependent on the contact pressure, over-closure and the average temperature at the contact point.

The heat flux due to radiation is found by the following relation:

$$q_r = F\left[(T_1 - T^Z)^4 - (T_2 - T^Z)^4\right], \tag{3.3}$$

where F is the gap radiation constant, T^Z is the absolute zero on the temperature scale used and T_1 and T_2 are the temperatures on surfaces 1 and 2, respectively.

Finally, the heat flux due to frictional heat generation is defined as follows:

$$q_g = \eta\tau\frac{\Delta s}{\Delta t}, \tag{3.4}$$

where η is the heat fraction, τ is the frictional stress, Δs is the incremental slip and Δt is the time step. ABAQUS/Explicit applies the Galerkin method to solve the set of equation for finding the total heat generated due to friction.

As for the heat generation due to plastic deformation, the plastic work caused by the accumulation of plastic strains converts into heat which, in turn, increases the heat flux per unit volume as follows:

$$r^{pl} = \beta\boldsymbol{\sigma} : \dot{\boldsymbol{\varepsilon}}^{pl}, \tag{3.5}$$

where β is the inelastic heat fraction which represents the percentage of the plastic work that is converted into heat inside the material, $\boldsymbol{\sigma}$ is the stress tensor and $\dot{\boldsymbol{\varepsilon}}^{pl}$ is the plastic strain increment tensor. The notation ":" is the double dot product of the two matrices which results in a scalar. The inelastic heat fraction is considered a constant throughout the analysis. The plastic strain rate is defined for plasticity models as:

$$\dot{\boldsymbol{\varepsilon}}^{pl} = \dot{\varepsilon}^{pl}\mathbf{n}, \tag{3.6}$$

where $\dot{\varepsilon}^{pl}$ is the equivalent plastic strain rate and $\mathbf{n}$ is the flow direction which is a function of stress, plastic strain and temperature. Newton-Raphson technique was utilized to solve the governing non-linear equations using the Backward Euler scheme as an integration tool. The dynamic flow stress of the material as

well as the damage evolution throughout the plastic deformation is predicted using the Johnson-Cook (JC) plasticity and dynamic failure models that are already implemented in ABAQUS/Explicit.

The JC dynamic flow stress is given by the following relation:

$$\sigma = \left[A + B(\overline{\varepsilon}^{pl})^n\right]\left[1 + C\ln\left(\frac{\dot{\overline{\varepsilon}}^{pl}}{\dot{\varepsilon}_o}\right)\right]\left(1 - \left(\frac{T - T_{\text{ref}}}{T_m - T_{\text{ref}}}\right)^m\right), \tag{3.7}$$

where A is the static yield strength, B is the strain hardening coefficient, $\overline{\varepsilon}^{pl}$ is the equivalent plastic strain, n is the strain hardening exponent, C is the strain rate sensitivity factor, $\dot{\overline{\varepsilon}}^{pl}$ is the equivalent plastic strain rate, $\dot{\varepsilon}_o$ is the reference strain rate, T is the temperature, T_{ref} is the reference room temperature, T_m is the melting temperature and m is the thermal sensitivity parameter. On the other hand, the damage evolution, ω, due to the accumulation of plastic strains inside the alloys is obtained using the following equation:

$$\omega = \sum\left(\frac{\Delta\overline{\varepsilon}^{pl}}{\overline{\varepsilon}_f^{pl}}\right), \tag{3.8}$$

where $\overline{\varepsilon}_f^{pl}$ is the plastic strain at failure defined as follows:

$$\overline{\varepsilon}_f^{pl} = \left[d_1 + d_2\exp\left(d_3\frac{p}{q}\right)\right]\left[1 + d_4\left(\frac{\dot{\overline{\varepsilon}}^{pl}}{\dot{\varepsilon}_o}\right)\right]\left[1 + d_5\left(\frac{T - T_{\text{ref}}}{T_m - T_{\text{ref}}}\right)\right], \tag{3.9}$$

where d_1 to d_5 are the failure parameters, p is the hydrostatic pressure and q is the Von Misses stress.

It should be emphasized that accurate description of the thermo-mechanical behavior of metals at high temperatures and strain rates is very crucial and requires microstructures-based constitutive relations. The empirical relation presented by the JC model was, however, used in this research because it is already implemented in ABAQUS and also for the availability of its parameters for AA5083. The authors are currently working on implementing the physically-based constitutive relations developed by Voyiadjis and Abed [18, 19] to describe the flow stress of the aluminum alloy or any other alloys (see for more details, ref. [20–22]).

3.2. Modeling

Finite element modeling of the friction stir welding process is a very complicated procedure as it involves excessive deformation accompanied with large amount of plastic straining and heat. Several attempts were made in this research

to simulate the FSW process efficiently and also to predict accurate temperature evolution throughout the deformation. The FE model was first generated using Lagrangian formulation for all of the three parts involved in the process; the tool, the aluminum plate and the backing plate. Both the tool and the backing plate were modeled as rigid bodies. The aluminum plate was merged with the backing plate. The tool was self-rotated, and the backing plate was modeled as a movable part to translate the welding plate in the welding direction. The plate was partitioned to refine the mesh in the stir zone in order to reduce the computational time. Tetrahedral 4-nod solid elements were utilized to model the large plastic deformation in the partitioned middle piece as shown in Fig. 4a; the rest of the plate, on the other hand, was modeled using 8-node linear brick elements. For such a model with a relatively high plastic deformation, a very fine mesh is required to avoid element distortion during the process. The very fine meshes as well as the high-frequency remeshing technique caused a drastic increase in the computational time. Attempt runs of this model on a high speed computer lasted for a very long period of time and didn't manage to model the first second of the process. With such an unrealistic computational time, the model was discarded even though it didn't experience any errors or crashes.

a) b)

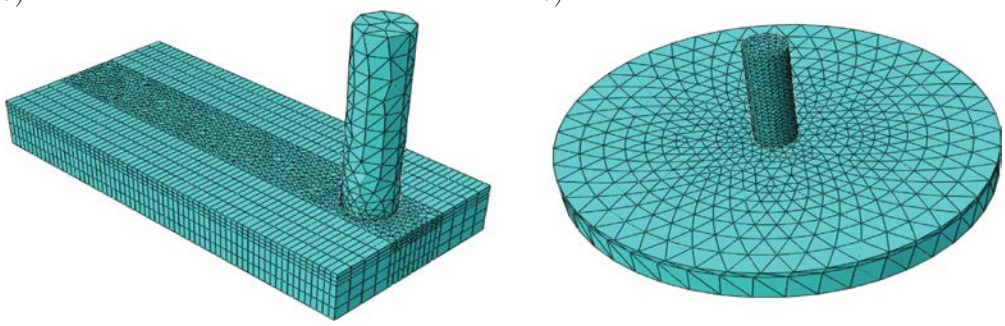

FIG. 4. Lagrangian-based FE models for friction process.

To eliminate the high aspect ratio problem for elements around the hole in a rectangular plate, the plate geometry was changed to a circular shape to achieve better meshing around the pin with uniform aspect ratios as shown in Fig. 4b. The computational cost was successfully reduced, as it took less time than the previous model. However, the run was aborted at less than 10% of the process due to excessive element distortion and no valuable results could be extracted.

To overcome the above-mentioned difficulties, Eulerian-Lagrangian formulation was, alternatively, adopted in the present FE analysis to model the FSW process using geometry similar to the one presented in Fig. 4a. The welding

plate was modeled using Eulerian part definition whereas; a Lagrangian part was assigned for the welding tool. Eulerian definition allows the material to flow through the mesh while the elements stay stationary and unaffected during the process. Moreover, using Eulerian elements eliminates any mesh distortions that occur during the process. The plate geometry is identical to the plates used in the experimental work, yet the welding tool was modified for simplicity. The welding plate was 130 mm in length, 60 mm in width and 4 mm in thickness. As for the welding tool, the diameter of the shoulder was 15 mm, and the diameter and length of the pin were 5 mm and 4 mm, respectively. Figure 5 shows the geometric description of the FE model used in the present analysis. More details about the FE modeling are given in the following subsections.

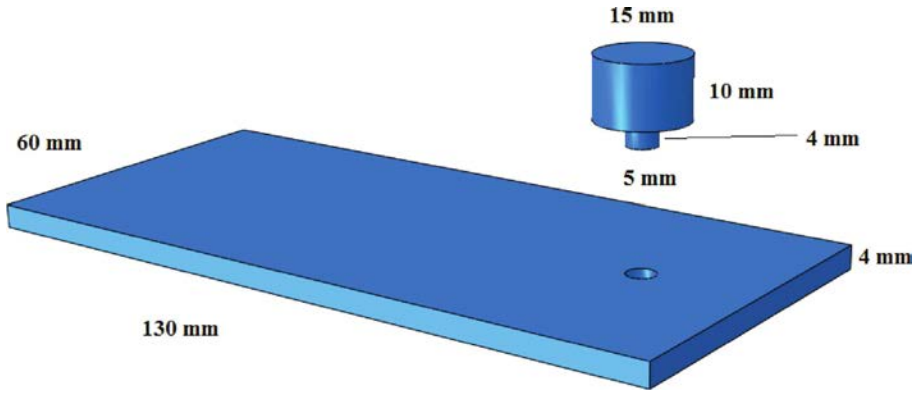

FIG. 5. Tool and plate geometry.

3.2.1. Material definition. The rotating tool was made of very high strength steel and was defined using Lagrangian formulation in the present FE simulations. The thermal conductivity used for steel was 45 W/(m·K) with a specific heat of 0.49 KJ/(Kg·K) at room temperature. The welding plate was made of 5083 aluminum alloy with a density of 2650 kg/m^3 and an elastic modulus of 72 GPa. The thermal conductivity of the alloy was set to 121 W/(m·K) with a specific heat equal to 0.91 KJ/(Kg·K) at room temperature. The thermo-viscoplastic behavior of aluminum alloy was defined using the Johnson-Cook (JC) flow stress model. Table 2 summarizes the JC model parameters for AA5083 which were collected from the literature [23].

Table 2. Experimental setup.

A [MPa]	B [MPa]	C	m	n	T_m [K]	T_r [K]
137.9	216.7	0.02	0.4845	1.225	933	293

3.2.2. Contact and boundary conditions. General contact definition was used to model the FSP process with a defined slipping condition. The maximum elastic slip used was 0.5% which is a default value defined by ABAQUS. The contact was defined in both normal and tangential directions of the plate. Hard contact definition was used in the normal direction and a penalty contact was adopted in the tangential direction, with a friction coefficient equal to 0.3 as recommended by previous research [14]. Heat generation due to friction was also defined and was distributed equally to each surface.

The bottom surface of the Eulerian welding plate was restrained from movement in all directions. A range of rotational speeds between 600 and 900 rpm was assigned to the tool, which was moving with a speed of 50 mm/min in the welding direction. The rigid tool was restrained from any rotation or movement in directions other than the previously specified. A predefined temperature field was also assigned to the welding plate and the tool to start the process at room temperature.

3.2.3. Mesh description. A total of 3200 8-node 3D solid elements were utilized to model the welding plate as depicted in Fig. 6. Adaptive Eulerian-

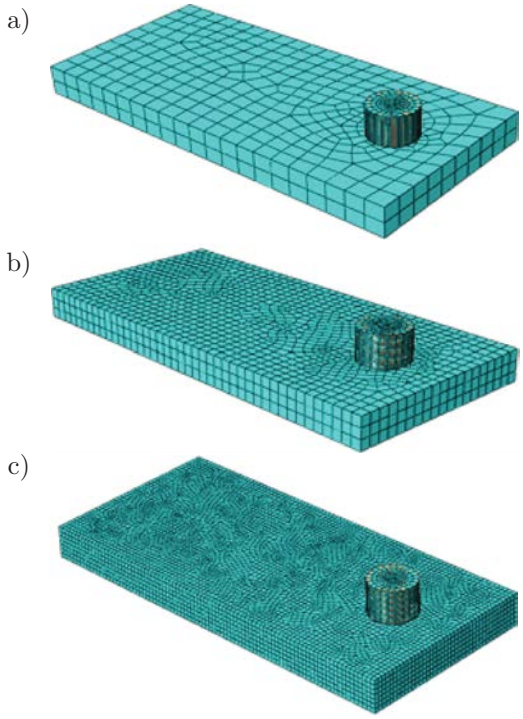

FIG. 6. Three mesh sizes used in the mesh sensitvity analysis a) coarse mesh, b) fine mesh and c) very fine mesh.

Lagrangian (ALE) meshing technique, which is very important for large deformation modeling, was also adopted to prevent any elements distortions during the process. When using Eulerian elements, a percentage of material is specified to fill each element. ALE technique allows the elements to start with 100% material and changes the percentage of material per element as the process goes on which allows the material to stir without causing any distortions or fictitious voids [16].

Mesh sensitivity analysis was also conducted to select a proper element size to accurately simulate the FSW process with a minimum computational cost. In this regard, three mesh sizes were considered; coarse mesh (Mesh A), fine mesh (Mesh B) and very fine mesh (Mesh C) as shown in Fig. 6. The peak temperatures obtained using these three meshes were compared with the experimental values as illustrated by the bar char shown in Fig. 7. FE modeling using Mesh A was found to overestimate the experimental peak temperature at the thermocouple location by more than 18%. On the other hand, the peak temperatures predicted using Mesh B and Mesh C were comparable with their experimental counterparts with a maximum difference of less than 4%. Mesh B was; therefore, selected in this study as it requires less computational time than Mesh C with nearly similar accuracy.

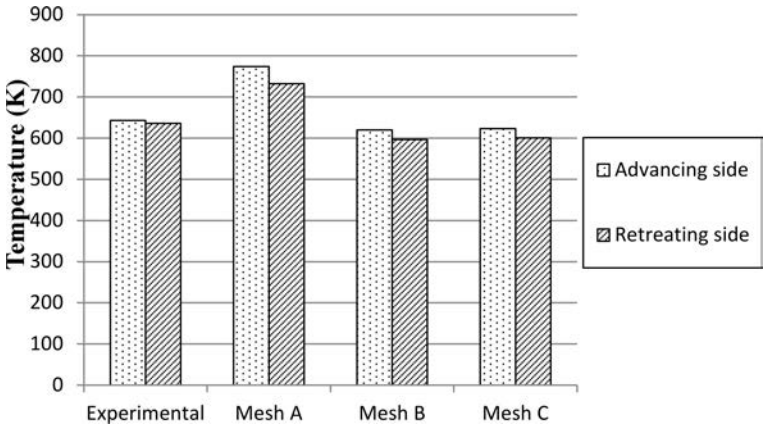

FIG. 7. Peak temperatures at the three different mesh sizes.

3.3. Results and discussion

The present FE model was verified against experimental results for FSP samples with similar conditions. The comparisons between the experiments and the FE analysis included: (a) the peak temperatures obtained at different rotational speed, (b) the difference in temperatures between the advancing and retreating sides, and (c) the thermal profile captured by the Infra-red camera.

The FE model was run at three different rotational speeds; 600 rpm, 700 rpm and 900 rpm. The resulting peak temperatures and thermal profiles encountered at these three speeds were compared with the results obtained experimentally. Figure 8 presents the variation of the peak temperatures with the rotational speeds as measured experimentally and predicted using the FE model. The FE model successfully predicted the temperature profiles of FSP at the three different rotational speeds. The peak temperature increased in the advancing and retreating sides as the rotational speed was raised, which is similar to the experimental results. The difference between the temperatures in the advancing and retreating sides predicted by the FE model was very close to the experimental results in all three rotational speeds.

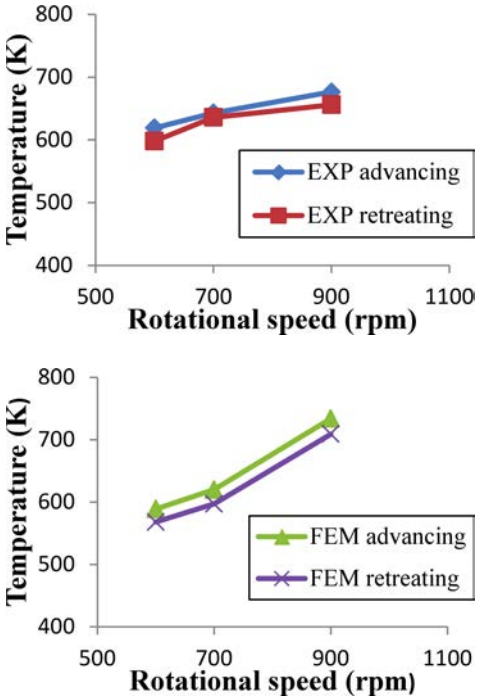

FIG. 8. Peak temperatures at the advancing and retreating sides found from experiments (top) and numerical model (bottom).

Figure 9 shows the thermal profile at the three different rotational speeds. The three thermal profiles are similar where the advancing side achieved higher temperatures than the retreating side. The figure also shows the increase in the overall temperature in addition to the peak temperatures as the rotational speed increases. The increase of heat generated is due to the increase of friction caused by raising the rotational speed of the tool.

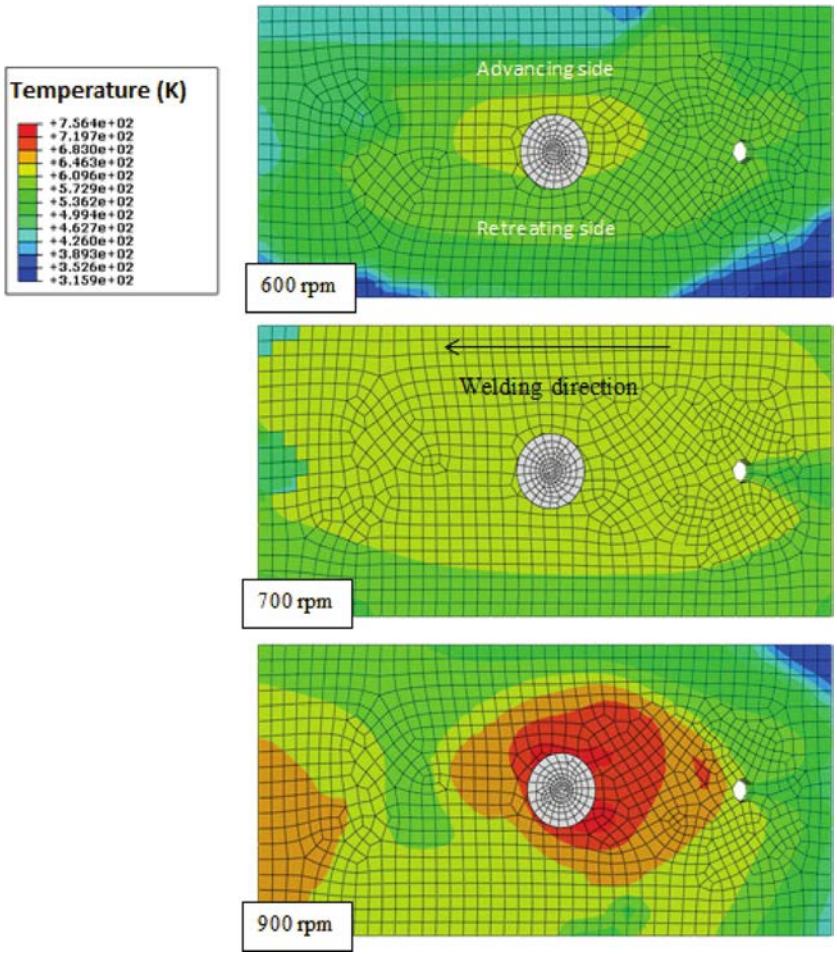

FIG. 9. Thermal profiles of FSP samples at 600 rpm (top), 700 rpm (middle) and 900 rpm (bottom).

Infrared images of FSP were also taken during the experiments to show the temperature profiles at different locations over the specimen. Samples of these images taken at two different locations are presented in Fig. 10 for the case of a rotational speed equal to 700 rpm. The FE model was able to predict similar temperature profiles to the ones captured by the IR camera for the same rotational speed as depicted in Fig. 11. The IR camera images were limited to a small diameter surrounding the tool as parts of the plate were hidden by the clamps holding it in the test setup. One advantage of the FE modeling is that the temperature profile can be observed over the whole plate which gives a better understanding of the thermal profile evolution during the FSP. As expected, the advancing side achieved higher peak temperature than the retreating side.

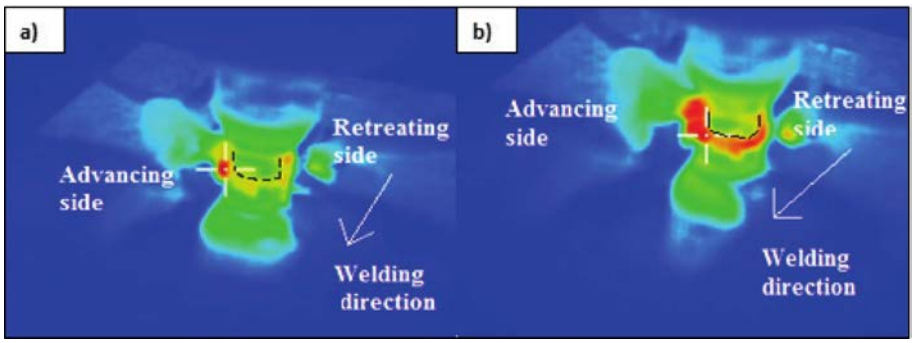

FIG. 10. Thermal profile captured by infrared camera at: a) beginning of FSP, b) halfway through FSP.

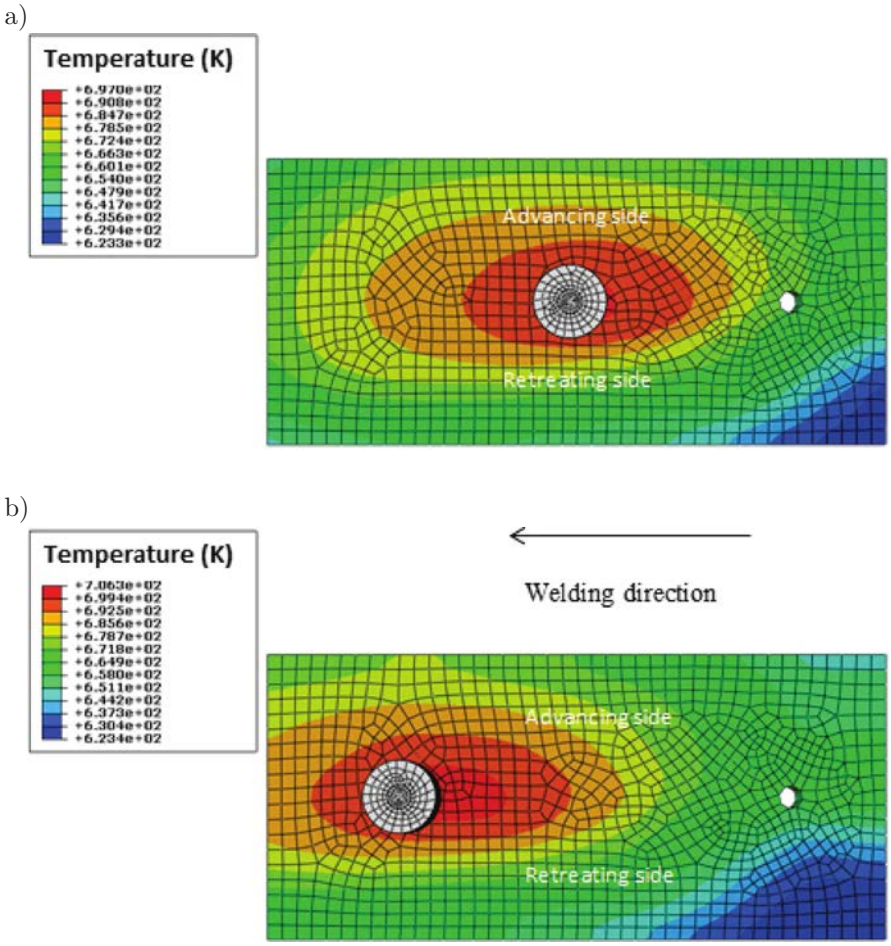

FIG. 11. Thermal profile predicted by FE model at: a) halfway through FSP and b) end of FSP.

It should be mentioned finally that the accuracy of the results presented in this research is limited to the accuracy of the selected flow stress model. The JC model used in this study is purely empirical, and its parameters depend merely on the set of the experimental data used for fitting. Consequently, extending the model application to a range of strain rates and temperatures beyond these data does not guarantee precise description of the plastic deformation. Therefore, it is recommended to use microstructures-based models that can accurately describe the coupling effect of temperature and strain rate on the material flow.

4. Conclusion

FSP was found difficult to model using Lagrangian finite element formulation as the high plastic deformation caused an excessive distortion in the mesh and increased the computational time drastically. Finite element simulation of the FSP was successfully achieved by adopting a coupled Eulerian Lagrangian formulation and by considering the thermo-mechanical behavior encountered during the friction process. The FE results were validated experimentally and a good agreement was achieved. The present Eulerian-based FE model was not only able to successfully predict the effect of rotational speeds on the peak temperature and thermal profiles in general, but was also capable of capturing the variation in thermal profiles between the advancing and the retreating sides. The present FE model can then be utilized to conduct an extensive parametric study to further investigate the various mechanical aspects accompanied by this complicated thermal process.

Acknowledgment

The support of the Emirates Foundation, Science and Engineering Research Grant # 2010/117, and the college of engineering at the American University of Sharjah are acknowledged.

References

1. Thomas W.M., Nicholas E.D., Needham J.C., Murch M.G., Temple Smith P., Dawes C.J., *Friction stir butt welding*, International patent application No. PCT/GB92/02203; December 1991.
2. Di Paola M., Falchero A., Cabibbo M., Evangelista E., Meccia E., Spigarelli S., *Mechanical and microstructural characterization of an Aluminum friction stir-welded butt joint*, Metallurgical Science and Technology, **20**, 17–21, 2002.
3. Lee W.B., Yeon Y.M., Jung S.B., *The improvement of mechanical properties of friction-stir-welded A356 Al alloy*, Materials Science and Engineering, **A355**, 154–159, 2003.

4. Jones M.J., Heurtier P., Desrayaud C., Montheillet F., Allehaux D., Driver J.H., *Correlation between microstructure and microhardness in a friction stir welded 2024 aluminium alloy*, Scripta Materialia, **52**, 693–697, 2005.

5. Darras B., Kishta E., *Submerged Friction Stir Processing of AZ31 Magnesium Alloy*, Material and Design, **47**, 133–137, 2012.

6. Colegrove P., Shercliff H., Zettler R., *A Model for Predicting the Heat Generation and Temperature in Friction Stir Welding from the Material Properties*, Science and Technology of Welding & Joining, **12**, 284–297, 2007.

7. Colegrove P., Shercliff H., *Two-dimensional CFD modelling of flow round profiled FSW tooling*, Science and Technology of Welding & Joining, **9**, 483–492, 2004.

8. Cho J-H., Dawson P., Boyce D., *2-D Modeling of Friction Stir Welding by Eulerian Formulation*, AIP Conf. Proc., **712**, 1326–1331, 2004.

9. Darras B., Khraisheh M., *Analytical Modeling of Strain Rate Distribution During Friction Stir Processing*, ASM Journal of Materials Engineering and Performance, **17**, 2, 168–177, 2008.

10. Darras B., *A Model to Predict the Resulting Grain Size of Friction-Stir-Processed AZ31 Magnesium Alloy*, ASM Journal of Materials Engineering and Performance, **21**, 7, 2012.

11. Buffa G., Hua J., Shivpuri R., Frantini L., *A continuum based fem model for friction stir welding – model development*, Material Science and Engineering, **A419**, 389–396, 2005.

12. Hamilton C., Sommers A., Dymek S., *A thermal model of friction stir welding applied to Sc-modified Al-Zn-Mg-Cu alloy extrusion*, International Journal of Machine Tools & Manufacture, **49**, 230–238, 2008.

13. Schmidt H., Hattel J., *A local model for the thermomechanical conditions in friction stir welding*, Modelling and Simulation in Materials Science and Engineering, **13**, 77–93, 2005.

14. ABAQUS/CAE Analysis User's Manual: version 6.11 (2011) by Abaqus.

15. Zhang Z., Zhang H.W., *Numerical studies on controlling of process parameters in friction stir welding*, Journal of Materials Processing Technology, **209**, 241–270, 2009.

16. Ulysse P., *Three-dimensional modeling of the friction stir-welding process*, International Journal of Machine Tools & Manufacture, **42**, 1549–1557, 2002.

17. Hofmann D.C., Vecchio K.S., *Submerged friction stir processing (SFSP): An improved method for creating ultra-fine-grained bulk materials*, Materials Science and Engineering, **A402**, 234–241, 2005.

18. Abed F.H., Voyiadjis G., *Adiabatic Shear Band Localizations in BCC Metals at High Strain Rates and Various Initial Temperatures*, International Journal for Multiscale Computational Engineering, **5**, 3–4, 2007.

19. Voyiadjis G., Abed F.H., *Transient Localizations in Metals Using Microstructure-based Yield Surfaces*, Modelling and Simulation in Materials Science and Engineering, **15**, 1, 2007.

20. Abed F.H., *Constitutive Modeling of the Mechanical Behavior of High Strength Ferritic Steels For Static and Dynamic Applications*, Mechanics of Time-Dependent Materials, **14**, 4, 329–345, 2010.

21. Abed F.H., Makarem F.S., *Comparisons of Constitutive Models For Steel Over a Wide Range of Temperatures and Strain Rates*, Journal of Engineering Materials and Technology-Transactions of the ASME, **134**, 2, 2012.

22. Abed F.H., *Physically Based Multiscale-Viscoplastic Model for Metals and Steel Alloys: Theory and Computation*, Doctoral dissertation, Louisiana State University.

23. Polyzois I., *Finite Element Modeling of the Behavior of Armor Materials Under High Strain Rates and Large Strains*, M.Sc. Thesis, University of Manitoba, Canada, 2010.